

Universal Behavior of Multipartite Entanglement in Crossing the Quantum Critical Point

Hao-Yu Sun,^{1,2} Zi-Yong Ge,^{3,*} and Heng Fan^{1,2,4,5,6,†}

¹*Beijing National Laboratory for Condensed Matter Physics,*

Institute of Physics, Chinese Academy of Sciences, Beijing 100190, China

²*School of Physical Sciences, University of Chinese Academy of Sciences, Beijing 100190, China*

³*Theoretical Quantum Physics Laboratory, RIKEN Cluster for Pioneering Research, Wako-shi, Saitama 351-0198, Japan*

⁴*Songshan Lake Materials Laboratory, Dongguan 523808, Guangdong, China*

⁵*CAS Center for Excellence in Topological Quantum Computation, UCAS, Beijing 100190, China*

⁶*Beijing Academy of Quantum Information Sciences, Beijing 100193, China*

(Dated: February 17, 2022)

We investigate multipartite entanglement of the quantum Ising model with transverse fields for a slow quantum quench crossing a critical point. The multipartite entanglement is quantified by quantum Fisher information with the generator defined as the operator of the ferromagnetic order parameter due to the system symmetry. The quench dynamics begin with the ground state of the large transverse field in the paramagnetic phase, and then the transverse field is driven slowly to cross a quantum critical point and ends with a zero transverse field. Based on methods of matrix product state, we calculate the quantum Fisher information density of the final state. Numerical results of both linear and nonlinear quench show that the quantum Fisher information density of the final state scales as a power law of the quench rate, which has an opposite exponent of the Kibble-Zurek scaling. Our results reveal that the multipartite entanglement provides a new viewpoint to understand the dynamics of quantum phase transition. Based on the observation of entanglement in the quenched state, we also expect that our result would inspire approaches for preparing multipartite entangled states in quantum information processing.

I. INTRODUCTION

Quantum entanglement plays a crucial role in quantum information processing and quantum computation. For instance, bipartite entanglement, generally represented by von Neumann or Rényi entropy, is an essential ingredient for supporting quantum advantages in quantum computation. Multipartite entanglement, quantified by spin squeezing or quantum Fisher information (QFI) [1–6], is an indispensable quantum resource to perform quantum metrology beyond standard quantum limit [7–12]. On the other hand, quantum entanglement can also be applied to understand quantum many-body physics [13–18]. Bipartite entanglement can be used to identify the different quantum phases and critical phenomena [19–21]. For example, there exists universal subleading entanglement entropy, termed topological entanglement entropy [19–22], in the intrinsic topological order system. In a critical system, the conformal field theory (CFT) predicts that the entanglement entropy is logarithmically divergent with respect to the system size, of which the factor is proportional to the central charge [23–25]. Recently, multipartite entanglement is also applied to witness the symmetry-protected topological order [26–29].

Kibble-Zurek mechanism (KZM) describes the universal dynamics of second-order phase transition. It is first proposed to understand the thermodynamic phase transition in cosmological physics [30, 31] and is also introduced to quantum many-body physics [32–44]. At the critical point, the correlation length and the relaxation time diverge, which is known as critical slowing down. Thus, for slow quench dynamics crossing a critical point, the adiabatic condition will break down, and the system can excite topological defects in the final state. KZM predicts that the density of topological defects n_d has a universal power law scaling with quench rate τ_Q : $n_d = \tau_Q^{-d\nu/(z\nu+1)}$ [30], where d is the system dimension, and ν and z are correlation length and dynamical critical exponents, respectively. Due to the fast development of technology in quantum simulations, KZM has been demonstrated experimentally in various synthetic quantum many-body systems [45–50].

In addition to the topological defects or energy production, KZM can be used to predict other physical quantities [51]. It is shown that the diagonal entropy after a slow quantum quench crossing the critical point also satisfies Kibble-Zurek scaling [52–55]. For the bipartite entanglement, von Neumann entropy is found to scale logarithmically with the quench rate, which is closely related to KZM [41, 56]. However, it is not clear the behaviors of multipartite entanglement relating to KZM in crossing the quantum critical point.

In this paper, we focus on the multipartite entanglement of the transverse field Ising model after a

* ziyong.ge@riken.jp

† hfan@iphy.ac.cn

slow quench crossing a quantum critical point. The multipartite entanglement is witnessed by QFI density, where the generator is the ferromagnetic order parameter. We calculate numerically the time evolution of the QFI density after a slow quench by matrix product state (MPS) based method. We find that the QFI density of the final state has a power-law scaling of the quench rate after both linear and nonlinear quench, where the exponent is opposite to the KZM scaling. In addition, based on the above results, we present a phenomenological description of critical slowing down in QPTs from the perspective of multipartite entanglement.

This paper is organized as follows: In Sec. II, we review the quantum Ising model with transverse fields including its spectrum and KZM. The multipartite entanglement and QFI are introduced in Sec. III. In Sec. IV, we study QFI of the final states after both linear and nonlinear quench. In Sec. V, we present a phenomenological discussion of our results. Finally, in Sec. VI, we summarize our results and present our outlook on further research. Additional details of the derivation are shown in Appendix A.

II. QUANTUM ISING MODEL AND KIBBLE-ZUREK MECHANISM

Here, we consider the one-dimensional spin- $\frac{1}{2}$ quantum Ising model with transverse fields, of which Hamiltonian reads

$$H = -J \sum_n \hat{\sigma}_n^z \hat{\sigma}_{n+1}^z - g \sum_n \hat{\sigma}_n^x, \quad (1)$$

where N is system size, $\hat{\sigma}^{x/z}$ is Pauli matrix, $J > 0$ is the nearest-neighbor interaction strength and is fixed to 1 in the following discussion, and g is the strength of transverse field. By Jordan-Wigner transformation, the Hamiltonian (1) can be written as a spinless fermionic form,

$$H = - \sum_n \left(\hat{c}_n^\dagger \hat{c}_{n+1} + \hat{c}_n \hat{c}_{n+1}^\dagger + h.c. \right) + \frac{g}{2} \sum_n \left(1 - 2\hat{c}_n^\dagger \hat{c}_n \right), \quad (2)$$

where \hat{c}_n (\hat{c}_n^\dagger) is the fermionic annihilate (create) operator at site n . If we choose periodic boundary condition for spin system, i.e., $\hat{\sigma}_{N+1} = \hat{\sigma}_1$, then it is periodic/anti-periodic boundary condition in fermionic system for odd/even fermion parity. Now we introduce a Fourier transform,

$$\hat{c}_n = \frac{1}{\sqrt{N}} \sum_k \hat{c}_k e^{ikn}, \quad (3)$$

where

$$k = \pm \frac{1}{2}, \dots, \pm \frac{N-3}{2}, \pm \frac{N-1}{2}. \quad (4)$$

Thus Hamiltonian (2) can be rewritten in momentum space as (where the constant term is neglected)

$$H = - \sum_k \left(e^{ik} \hat{c}_k^\dagger \hat{c}_k + e^{-ik} \hat{c}_k \hat{c}_{-k} + h.c. \right) - g \sum_k \hat{c}_k^\dagger \hat{c}_k. \quad (5)$$

By Bogoliubov transformation

$$\hat{c}_k = u_k \hat{\gamma}_k + v_k \hat{\gamma}_{-k}^\dagger, \quad (6)$$

the Hamiltonian (5) can be diagonalized as

$$\begin{pmatrix} g - \cos k & \sin k \\ \sin k & -g + \cos k \end{pmatrix} \begin{pmatrix} u_k \\ v_k \end{pmatrix} = \varepsilon_k \begin{pmatrix} u_k \\ v_k \end{pmatrix}. \quad (7)$$

The mode $(u_k, v_k)^\text{T}$ is the eigenstate of the Bogoliubov-de Gennes (B-dG) equation with eigenvalue

$$\varepsilon_k = \pm \sqrt{(g - \cos k)^2 + \sin^2 k}. \quad (8)$$

When $|g| = g_c = 1$, the system is gapless and thus locates at the critical point. When $|g| > g_c$, the spins tend to polarize in x -direction at the ground state, so the system is in the paramagnetic phase. When $|g| < g_c$, the system emerges long-range order, i.e., in ferromagnetic phase.

Now, we consider a slow quench dynamics of the quantum Ising model. Here, the transverse field is time-dependent and satisfying

$$g(t) = -t/\tau_Q + 1, \quad (9)$$

where $-\infty \leq t \leq \tau_Q$. The initial state is the ground state of $g = \infty$, i.e. all spins are polarized to the ground state of $-\hat{\sigma}_n^x$. During the slow quench to zero transverse field, the system needs to cross the critical point and the adiabaticity breaks. We label the instantaneous eigenstate at time t as $|\psi(t)\rangle$. Thus, the final state can be denoted as $|\psi(\tau_Q)\rangle$, which can be regarded as the state annihilated by operators following $\tilde{\gamma}_k |\psi(\tau_Q)\rangle = 0$. Here $\tilde{\gamma}_k$ is defined by the time dependent Bogoliubov transformation

$$\hat{c}_k = u_k(t) \tilde{\gamma}_k + v_k(t) \tilde{\gamma}_{-k}^\dagger, \quad (10)$$

where $[u_k(t), v_k(t)]^\text{T}$ is the eigenstate of dynamical B-dG equations. Since k -mod is decoupled to each other, the dynamical BdG equation can be mapped into a Landau-Zener (LZ) problem [39–41]. Thus, we have the excitation probability of a k -mode as [38]

$$p_k = e^{-\frac{2\pi\tau_Q k^2}{\hbar}}. \quad (11)$$

The topological density of the final state is the summation of all k , i.e., $n_d = \sum_k p_k$. In the thermodynamic limit $N \rightarrow \infty$, it is obtained by a Gaussian integral as

$$n_d = \frac{1}{2\pi} \int_{-\pi}^{\pi} p_k dk = \frac{1}{2\pi} \sqrt{\frac{\hbar}{2J\tau_Q}}. \quad (12)$$

This result reveals that the topological defect density has a power law scaling with respect to the quench rate [38],

$$n_d \sim \tau_Q^{-1/2}. \quad (13)$$

To understand this result, we need to introduce KZM [18, 37]. The excitation can be only excited around the critical point, where the adiabatic approximation breaks down. The coherence time is determined by the inverse of the energy gap, i.e., $\tau \sim \Delta^{-1}$. The adiabatic condition fails at $\tau \sim \hat{t}$, which is determined by

$$\hat{t} = |\dot{\Delta}/\Delta|, \quad (14)$$

where $\Delta \sim |g - g_c|^{z\nu} = |t/\tau_Q|^{z\nu}$. The solution reads

$$\hat{t} \sim \tau_Q^{z\nu/z\nu+1}, \quad (15)$$

and the corresponding energy gap scales as

$$\hat{\Delta} \sim \tau_Q^{-z\nu/z\nu+1}. \quad (16)$$

Therefore, the excitation density scales

$$n_d \sim \hat{\Delta}^{d/z} \sim \tau_Q^{-d\nu/z\nu+1}, \quad (17)$$

where d is the system dimension. This is known as KZM.

III. QUANTUM FISHER INFORMATION AND MULTIPARTITE ENTANGLEMENT

Generally, given an operator \hat{O} and a quantum state with density matrix $\hat{\rho} = \sum_i p_i |\psi_i\rangle\langle\psi_i|$, where $\langle\psi_i|\psi_j\rangle = \delta_{ij}$ and p_i is the probability, the corresponding QFI can be defined as

$$F_Q := 2 \sum_{p_i + p_j \neq 0} \frac{(p_i - p_j)^2 |\langle\psi_i|\hat{O}|\psi_j\rangle|^2}{p_i + p_j}. \quad (18)$$

For a pure state $\hat{\rho} = |\psi\rangle\langle\psi|$, QFI can be simplified as

$$F_Q = 4(\Delta\hat{O})^2 = 4(\langle\psi|\hat{O}^2|\psi\rangle - \langle\psi|\hat{O}|\psi\rangle^2). \quad (19)$$

In addition, we can define the QFI density of a system with N particles as

$$f_Q = \frac{1}{N} F_Q. \quad (20)$$

The physical significance of QFI density is that there are at least $[f_Q] + 1$ particles entangled [57], where $[f_Q]$ represents the maximum integer that is smaller than f_Q . That is, QFI is a quantification of multipartite entanglement. Generally, QFI or multipartite entanglement is an important quantum resource in quantum metrology, which quantifies the maximal precision of parameter estimation. Recently, multipartite entanglement is also applied to understand quantum many-body physics, e.g.,

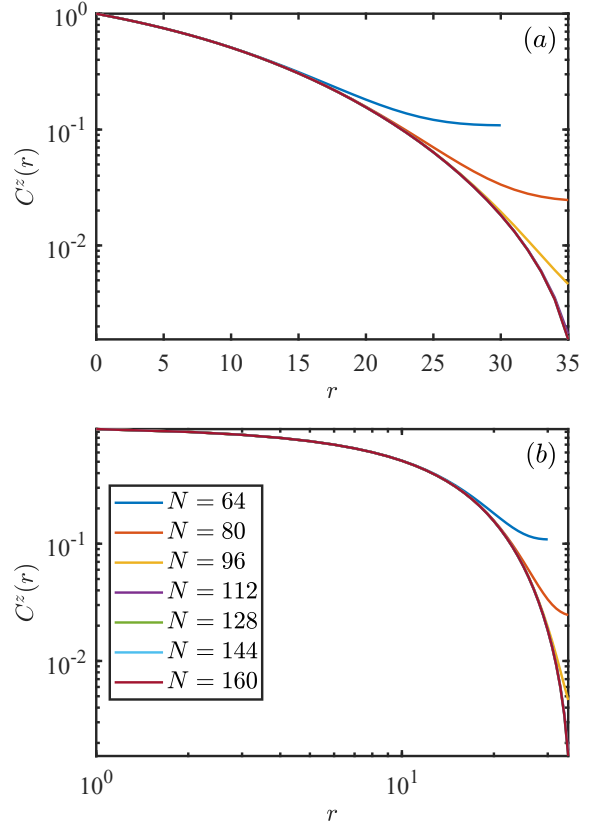


FIG. 1. Correlation functions of the final state after a linear quench for different sizes with (a) linear-logarithmic axis and (b) logarithmic-logarithmic axis. Here, the corresponding quench rate is $\tau_Q = 20$. To avoid the boundary effect, we fix one operator at the central position of the lattice, i.e., $C^z(r) = \langle \hat{\sigma}_{L/2}^z \hat{\sigma}_{L/2+r}^z \rangle$.

as a witness of topological phase [26, 29]. It is known that bipartite entanglement, generally represented by von Neumann or Rényi entropy, is closely related to QPTs [9]. One may wonder whether the scaling behaviors of multipartite entanglement quantified by QFI can be described as KZM. Next, we will study the QFI of the final state quenched from the polarized state crossing the critical point with the rate τ_Q .

IV. QUANTUM FISHER INFORMATION AFTER A SLOW QUANTUM QUENCH

Now we start to investigate multipartite entanglement of transverse Ising model after a slow quantum quench, i.e., considering the dynamics of following time-dependent Hamiltonian

$$H(t) = - \sum_{n=1} \hat{\sigma}_n^z \hat{\sigma}_{n+1}^z - g(t) \sum_{n=1} \hat{\sigma}_n^x. \quad (21)$$

We begin with a ground state of large g in the paramagnetic phase and mainly concern the relation between QFI density and quench rate. Generally, QFI depends on the corresponding generator \hat{O} , so we first need to choose a proper operator in Eq. (19). For $\hat{H}(t)$, there is a global \mathbb{Z}_2 spin-flip symmetry, of which transformation operator has the form

$$\hat{P} = \prod_{n=1}^N \hat{\sigma}_n^x. \quad (22)$$

Here, the initial state is a ground state of the paramagnetic phase, which is \mathbb{Z}_2 symmetry unbroken. In addition, we consider an isolated system, so the final state after the quench dynamics is also symmetry unbroken. For the final Hamiltonian, i.e., $g = 0$, the corresponding symmetry unbroken ground state is a GHZ state

$$\frac{1}{\sqrt{2}} (|\uparrow\rangle^{\otimes N} + |\downarrow\rangle^{\otimes N}), \quad (23)$$

which has the maximum QFI density N with respect to the operator $\hat{O} = \sum_{n=1}^N \hat{\sigma}_n^z$. Assuming that the quench is slow enough, we expect that the final state will be very close to the GHZ state. Based on these considerations, we can choose the operator as $\hat{O} = \sum_{n=1}^N \hat{\sigma}_n^z$ to calculate QFI.

According to Eq. (19) and since $\langle \hat{\sigma}_n^z \rangle = 0$ (due to the existence of spin-flip symmetry.), we can calculate QFI density as

$$f_Q = \frac{1}{N} \left\langle \left(\sum_{n=1}^N \hat{\sigma}_n^z \right)^2 \right\rangle = \frac{1}{N} \sum_{m=1}^N \sum_{n=1}^N \langle \hat{\sigma}_m^z \hat{\sigma}_n^z \rangle, \quad (24)$$

where $\langle \cdot \rangle$ means the expectation value with respect to the final state. Now, one can find that f_Q is the summation of two-site spin-spin correlation function of each pair. In the thermodynamic limit, i.e., $N \rightarrow \infty$, f_Q of the final state is

$$f_Q = 1 + \sum_{r=1}^N C_z(r), \quad (25)$$

where $C_z(r) = \langle \hat{\sigma}_i^z \hat{\sigma}_{i+r}^z \rangle$ is the correlation function with distance r .

Here, we adopt MPS based method to study the slow quench dynamics with open boundary conditions. Firstly, we apply the DMRG algorithm to obtain the ground state for $g = 5$ as the initial state. Then, utilizing time-evolving block decimation (TEBD) algorithm [58–62], we can calculate the wave function of the final state. Thus, according to Eq. (24), we can obtain the QFI density of the final state. For DMRG calculation, the maximum bond dimension is 100 with truncation error smaller than 10^{-12} . For TEBD calculation, we choose second-order Suzuki-Trotter decomposition. Furthermore, we also

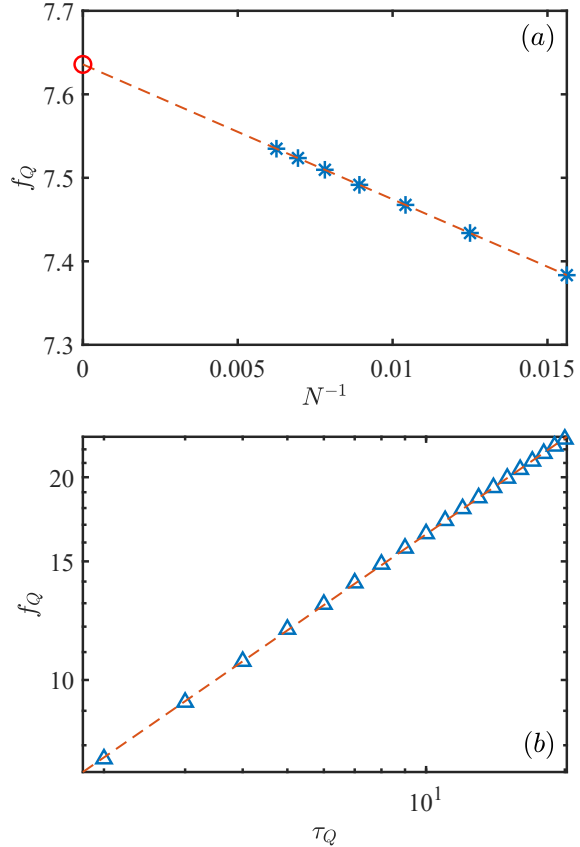


FIG. 2. The QFI density f_Q after linear quenches crossing a quantum critical point. (a) Finite-size scaling of the QFI density of the final state $\tau_Q = 2$. The scatters are results of fixed finite size calculated by MPS based method, while the dashed line is the fitting curve. It indicates that $f_Q \approx f_Q^\infty - A/N$, where the intercept f_Q^∞ (red circle) can be considered as the QFI density in the thermodynamic limit. Here, we obtain the interception value of about 7.6358. (b) The relation between QFI density f_Q and quench rate τ_Q in the thermodynamic limit. Each scatters is obtained by the method shown in (a). The dashed line is the linear fitting curve. It is shown that f_Q exhibits a power law scaling with respect to τ_Q , where the fitting result is $f_Q \sim \tau_Q^{0.474 \pm 0.002} \sim \tau_Q^{1/2}$.

enlarge the maximum bond dimension and decrease the time of a single step to increase the precision of results, where the truncation error is smaller than 10^{-11} and the minimum time step of Suzuki-Trotter decomposition is $\delta t = 0.02$.

A. Linear quench

Since the adiabatic condition breaks only in the vicinity of the critical point, only the quench rate at

t_c (where $g(t_c) = g_c = 1$), i.e., $g'(t_c)$, dominates the transition from ground state to excited states. That is, if the derivative of $g(t)$ at t_c is a finite value, $g(t)$ can be replaced by a linear function with slope $g'(t_c)$. Thus, following the progress of conventional KZM in quantum Ising model, we first consider a linear slow quench. Thus, the time-dependent transverse field has the form

$$g(t) = -\frac{t}{\tau_Q} + 1, \quad -4\tau_Q \leq t \leq \tau_Q, \quad (26)$$

where τ_Q represents the quench rate and $t_c = 0$. The whole quench dynamics begins with $g = 5$ and ends with $g = 0$.

In Fig. 1, we present the correlation function $C_z(r)$ of the final state. It is shown that $C_z(r)$ decays very quickly as the increase of distance r , even faster than the exponential law [41]. Thus, the final state has no long-range correlation. Now we start to consider the QFI density f_Q of the final state. To obtain more precise f_Q in the thermodynamic limit, we first calculate f_Q for a fixed τ_Q with different system sizes, and then we use finite-size scaling to fit out f_Q for $N \rightarrow 0$, see Fig. 2(a). Finally, we study the relation between f_Q and quench rate τ_Q . From Fig. 2(b), we can find that $f_Q \sim \tau_Q^{0.47} \approx \tau_Q^{1/2}$. Therefore, the number of entangled spins after a slow quench has a power-law scaling with respect to the quench rate.

As mentioned in Sec. II, the conventional KZM predicts that the topological defect density of final state satisfying the scaling $n_d \sim \tau_Q^{-d\nu/(z\nu+1)}$. For transverse Ising model, the topological defect is the domain wall $n_d(i) := \frac{1}{2}(1 - \langle \hat{\sigma}_i^z \hat{\sigma}_{i+1}^z \rangle)$ and $d = \nu = z = 1$, so $n_d \sim \tau_Q^{-\frac{1}{2}}$. Therefore, after a linear quench, the QFI density f_Q has the inverse scaling to one of the topological defects.

Now we try to understand the above result. For QFI density, according to the behavior of correlation function $C_z(r)$, we can find the main contributions to f_Q originate from $C_z(r < \xi)$, where ξ can be regarded as the correlation or coherence length of the final state. That is, QFI density is the reflection of the correlation length. Generally, after a linear quench crossing critical point, the correlation length is the inverse of topological defect density, i.e., $\xi \sim \tau_Q^{\nu/(z\nu+1)}$ [41]. Therefore, the scaling of QFI density should satisfy

$$f_Q \sim \tau_Q^{d\nu/(z\nu+1)}, \quad (27)$$

which is consistent with the numerical results.

B. Nonlinear quench

To further illustrate the results in Eq. (27), we study the QFI density after a nonlinear quench. Generally, if the

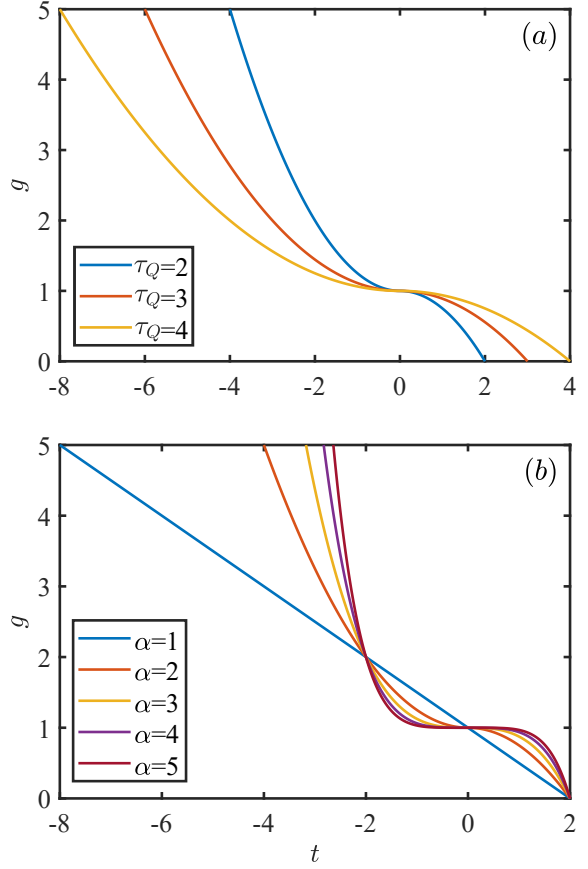


FIG. 3. Transverse field g driven versus time t for nonlinear quench. (a) Fixed $\alpha = 2$ with different quench rates and (b) fixed $\tau_Q = 2$ with different α .

derivative of $g(t)$ is zero at t_c , then the approximation of the linear quench is invalid. For this type of nonlinear quench, we can apply Taylor expansion and use the leading term to describe this nonlinear quench dynamics. Hence, we can use the following power law function to study the general nonlinear quench

$$g(t) = -\text{sgn}(t) \left| \frac{t}{\tau_Q} \right|^\alpha + 1.. \quad (28)$$

where $\alpha > 0$, see Fig. 3. In addition, similar to the linear case, the nonlinear quench dynamics begins with $g = 5$ and ends with $g = 0$.

Here, the nonlinear quench of Eq. (28) can be considered as a linear quench with respect to the driven parameter $\lambda = (g - 1)^{1/\alpha}$ with the critical exponents

$$z_\lambda = z = 1, \quad \nu_\lambda = \alpha\nu = \alpha. \quad (29)$$

The detailed analysis is presented in Appendix A. Therefore, according to Eqs (27) and (29), the QFI

density of the final state after a nonlinear quench, labeled f_Q^{nl} , should have the form

$$f_Q^{\text{nl}} \sim \tau_Q^{d\nu_\lambda/(z_\alpha\nu_\lambda+1)} = \tau_Q^{\alpha/(\alpha+1)}. \quad (30)$$

We note that the scaling behavior of topological defects after a nonlinear quench has been studied in Refs [41, 42], where the results are consistent with ours.

In Fig. 4, we present the numerical results of QFI density. According to Fig. 4(a), we can find that f_Q^{nl} indeed exhibits a power law relation with τ_Q . By linear fittings, we can obtain the corresponding power-law indexes for different α , which is consistent with Eq (30), see Fig. 4(b). These results further demonstrate the validity of Eq. (27).

V. DISCUSSION

Generally, near the critical point, the relaxation time of the system is divergent, where the divergent exponent depends on critical exponents. This phenomenon is known as critical slowing down, which can be regarded as the origin of KZM. Here, based on the above results, we try to understand the phenomenon of critical slowing down in QPTs from the viewpoint of multipartite entanglement.

For a local quantum many-body system, due to the Lieb-Robinson bounds [63, 64], the minimum time it takes to create a state with extended multipartite entanglement from a short-range entangled state scales linearly in the size of the system. That is if the local system size is N and the QFI density of the initial state is $O(1)$, then the time cost for creating a state with QFI density proportional to N is at least $\propto N$. In our system, for the linear quench, if we want $f_Q \propto N$ for the final state, then the quench rate $\tau_Q \propto N^2$. Thus, we need time $t \propto N^2$ to create a state with extended QFI density via a linear quench crossing a QPT, which is slower than the adiabatic case. Furthermore, in the case of nonlinear quench, the corresponding time cost is $N^{\frac{\alpha+1}{\alpha}} > N$. Only if $\alpha \rightarrow \infty$, which is equivalent to an adiabatic process, the rate of increasing QFI is identical to the adiabatic case.

Therefore, compared with the adiabatic process, the rate of generating multipartite entanglement near the critical point becomes slow and is closely related to the critical exponents. This behavior of multipartite entanglement crossing a QPT can be considered as a reflection of critical slowing down.

VI. SUMMARY AND OUTLOOK

In summary, we have studied the multipartite entanglement after slow quantum quenches crossing a QPT.

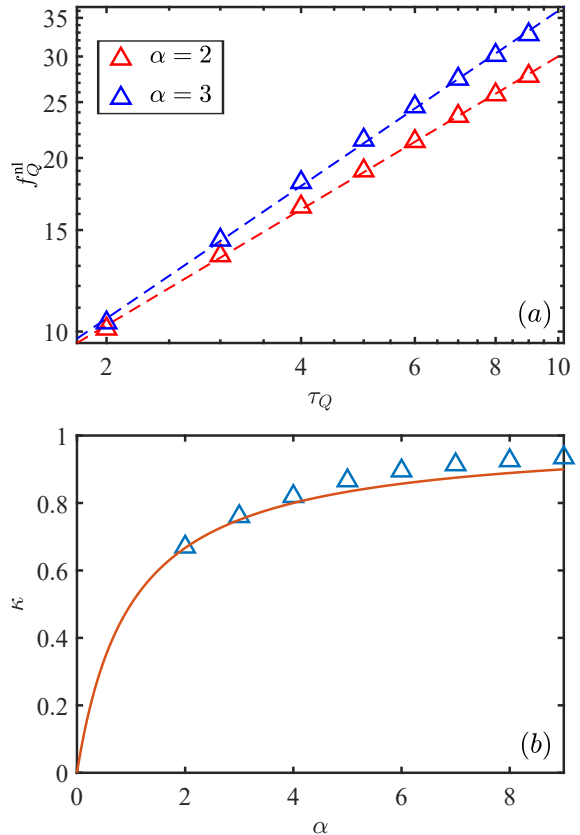


FIG. 4. The QFI density f_Q^{nl} after nonlinear quenches crossing a quantum critical point. (a) The relations between QFI density f_Q^{nl} and quench rate τ_Q in the thermodynamic limit for different α . Each scatters is obtained by the finite-size scaling in Fig. 2(a), and the dashed line is the linear fitting curve. The fitting result is $f_Q^{\text{nl}} \sim \tau_Q^{0.66 \pm 0.02} \sim \tau_Q^{2/3}$ for $\alpha = 2$ and $f_Q^{\text{nl}} \sim \tau_Q^{0.76 \pm 0.02} \sim \tau_Q^{3/4}$ for $\alpha = 3$. (b) The relation between scaling exponent of f_Q^{nl} (labeled by κ) and α . Each scatters is the fitted results of the power-law scaling exponent for different α . The orange solid curve is the function image of $\kappa(\alpha) = \frac{\alpha}{\alpha+1}$.

By numerical calculations via MPS-based methods, we find that the QFI density of the final state follows the scaling behavior opposite to the one in KZM. Our results reveal that KZM can not only predict the topological defect density but also the multipartite entanglement after crossing a QPT. Moreover, these results can also help us understand QPTs and the behavior of critical slowing down in another viewpoint, i.e., from the perspective of multipartite entanglement. In addition, since QFI is accessible in quantum simulation experiments, we expect that our results can be realized experimentally in state-of-art quantum simulators.

There also remain many interesting open questions, which are deserved to be further studied. In this work,

we only consider the 1D system, and it is meaningful to generalize our results to higher-dimensional systems to verify whether QFI density still satisfies the conventional KZM $f_Q \sim \tau_Q^{d\nu/z\nu+1}$. Moreover, when calculating QFI density, we choose the corresponding local operator based on the symmetry of the Hamiltonian. In this system, the QPT originates from a spontaneous symmetry breaking, so we can use the order parameter to define QFI. Therefore, it will be an interesting issue to study multipartite entanglement after slow quantum quenches crossing a topological QPT, which is absent of spontaneous symmetry breaking.

ACKNOWLEDGMENTS

I would like to thank Yu-Ran Zhang and Rui-Zhen Huang for helpful discussions. In this work, the numerical results are obtained by Tensor Network Python (TeNPy). This work is supported by the National Natural Science Foundation of China (Grants Nos. 11934018, T2121001), Strategic Priority Research Program of Chinese Academy of Sciences (Grant No. XDB28000000), Scientific Instrument Developing Project of Chinese Academy of Sciences (Grant No. YJKYYQ20200041) and Beijing Natural Science Foundation (Grant No. Z200009).

Appendix A: Topological defect with a nonlinear exponent

Here, we show how to understand nonlinear quench in the viewpoint of parameter-dependent critical exponents. Generally, the definition of the critical exponents depends on the driven parameter. For instance, the correlation length and dynamical exponents of quantum Ising model

with respective to transverse field g can be defined as

$$\begin{aligned}\xi &\sim |g - g_c|^{-\nu}, \\ \Delta &\sim |g - g_c|^{z\nu},\end{aligned}\quad (\text{A1})$$

where g is in the vicinity of g_c , and Δ is the energy gap. Now, we assume the transverse field g is a function of an another parameter λ , i.e., $g = g(\lambda)$. Here, we let $g_c = g(\lambda_c)$, and without generality, we fix $\lambda_c = 0$. Thus, Eq. (A1) can be rewritten as

$$\begin{aligned}\xi &\sim |g(\lambda) - g(\lambda_c)|^{-\nu} \sim |\lambda g'(\lambda)|^{-\nu}, \\ \Delta &\sim |g(\lambda) - g(\lambda_c)|^{z\nu} \sim |\lambda g'(\lambda))|^{z\nu},\end{aligned}\quad (\text{A2})$$

where $g(\lambda_c) = g_c$. In addition, if we consider λ as the driven parameter of the QPT, where λ_c is the critical point, then the corresponding critical exponents, labeled as ν_λ and z_λ , can be defined as

$$\begin{aligned}\xi &\sim \lambda^{-\nu_\lambda}, \\ \Delta &\sim \lambda^{z_\lambda \nu_\lambda}.\end{aligned}\quad (\text{A3})$$

According to Eqs. (A1, A3), when $g'(\lambda_c) = 0$, we can find that $\nu_\lambda = \nu$ and $z_\lambda = z$. However, if $g'(\lambda_c) \neq 0$, the situation is different. For the nonlinear quench in the main text, we have

$$g(t) = -\text{sgn}(t)|t/\tau_Q|^\alpha + 1. \quad (\text{A4})$$

If we let $\lambda = (g - 1)^{1/\alpha}$, then $g(\lambda) = \lambda^\alpha + 1$. Thus, in the vicinity of λ_c , we can calculate the derivative of $g(\lambda)$ as $g'(\lambda) = \alpha \lambda^{\alpha-1}$. Therefore, from Eqs. (A1, A2), we can obtain the critical exponents with respective to λ as

$$\begin{aligned}\nu_\lambda &= \alpha \nu, \\ z_\lambda &= z.\end{aligned}\quad (\text{A5})$$

In addition, we have $\lambda(t) = t/\tau_Q$. Thus, this nonlinear quench with respective to g is transformed into a linear quench for λ , where the results of linear quench can be applied directly in this case. For instance, we can use KZM to obtain the topological defects density of the final state after as

$$n_d \sim \tau_Q^{-d\nu_\lambda/(z\nu_\lambda+1)} = \tau_Q^{-\alpha/(\alpha+1)}, \quad (\text{A6})$$

which is consistent with the result in Refs [41, 42].

[1] Y.-R. Zhang, Y. Zeng, H. Fan, J. You, and F. Nori, Characterization of Topological States via Dual Multipartite Entanglement, *Phys. Rev. Lett.* **120**, 250501 (2018).

[2] P. Hyllus, W. Laskowski, R. Krischek, C. Schwemmer, W. Wieczorek, H. Weinfurter, L. Pezzé, and A. Smerzi, Fisher information and multiparticle entanglement, *Phys. Rev. A* **85**, 022321 (2012).

[3] G. Tóth, Multipartite entanglement and high-precision metrology, *Phys. Rev. A* **85**, 022322 (2012).

[4] L. Pezzé, M. Gabelli, L. Lepori, and A. Smerzi, Multipartite Entanglement in Topological Quantum Phases, *Phys. Rev. Lett.* **119**, 250401 (2017).

[5] P. Hauke, M. Heyl, L. Tagliacozzo, and P. Zoller, Measuring multipartite entanglement through dynamic susceptibilities, *Nat. Phys.* **12**, 778 (2016).

[6] L.-A. Wu, S. Bandyopadhyay, M. S. Sarandy, and D. A. Lidar, Entanglement observables and witnesses for interacting quantum spin systems, *Phys. Rev. A* **72**, 032309 (2005).

[7] S. L. Braunstein and C. M. Caves, Statistical distance and the geometry of quantum states, *Phys. Rev. Lett.* **72**, 3439 (1994).

[8] V. Giovannetti, S. Lloyd, and L. Maccone, Quantum Metrology, *Phys. Rev. Lett.* **96**, 010401 (2006).

[9] L. Pezzè, Y. Li, W. Li, and A. Smerzi, Witnessing entanglement without entanglement witness operators, *Proc. Natl. Acad. Sci.* **113**, 11459 (2016).

[10] V. Giovannetti, S. Lloyd, and L. Maccone, Advances in quantum metrology, *Nat. Photonics* **5**, 222 (2011).

[11] Y. Peng and H. Fan, Feedback ansatz for adaptive-feedback quantum metrology training with machine learning, *Phys. Rev. A* **101**, 022107 (2020).

[12] Z.-A. Wang, Y. Peng, D. Yu, and H. Fan, Beating standard quantum limit via two-axis magnetic susceptibility measurement, *Chin. Phys. B* (2021).

[13] Y. Xia, D. Qian, D. Hsieh, L. Wray, A. Pal, H. Lin, A. Bansil, D. Grauer, Y. S. Hor, R. J. Cava, and M. Z. Hasan, Observation of a large-gap topological-insulator class with a single Dirac cone on the surface, *Nat. Phys.* **5**, 398 (2009).

[14] L. Amico, R. Fazio, A. Osterloh, and V. Vedral, Entanglement in many-body systems, *Rev. Mod. Phys.* **80**, 517 (2008).

[15] B. Zeng, X. Chen, D.-L. Zhou, and X.-G. Wen, *Quantum Information Meets Quantum Matter* (Springer New York, 2019).

[16] K. Xu, J.-J. Chen, Y. Zeng, Y.-R. Zhang, C. Song, W. Liu, Q. Guo, P. Zhang, D. Xu, H. Deng, K. Huang, H. Wang, X. Zhu, D. Zheng, and H. Fan, Emulating Many-Body Localization with a Superconducting Quantum Processor, *Phys. Rev. Lett.* **120**, 050507 (2018).

[17] S. Sachdev, *Quantum Phase Transitions* (Cambridge University Press, 2009).

[18] S. Suzuki, J. ichi Inoue, and B. K. Chakrabarti, *Quantum Ising Phases and Transitions in Transverse Ising Models* (Springer Berlin Heidelberg, 2013).

[19] A. Kitaev and J. Preskill, Topological Entanglement Entropy, *Phys. Rev. Lett.* **96**, 110404 (2006).

[20] M. Levin and X.-G. Wen, Detecting Topological Order in a Ground State Wave Function, *Phys. Rev. Lett.* **96**, 110405 (2006).

[21] H. Li and F. D. M. Haldane, Entanglement Spectrum as a Generalization of Entanglement Entropy: Identification of Topological Order in Non-Abelian Fractional Quantum Hall Effect States, *Phys. Rev. Lett.* **101**, 010504 (2008).

[22] J. Eisert, M. Cramer, and M. B. Plenio, Colloquium: Area laws for the entanglement entropy, *Rev. Mod. Phys.* **82**, 277 (2010).

[23] G. Vidal, J. I. Latorre, E. Rico, and A. Kitaev, Entanglement in Quantum Critical Phenomena, *Phys. Rev. Lett.* **90**, 227902 (2003).

[24] C. Holzhey, F. Larsen, and F. Wilczek, Geometric and renormalized entropy in conformal field theory, *Nucl. Phys. B* **424**, 443 (1994).

[25] J. Cardy, Quantum quenches to a critical point in one dimension: some further results, *J. Stat. Mech: Theory Exp.* **2016**, 023103 (2016).

[26] A. Osterloh, L. Amico, G. Falci, and R. Fazio, Scaling of entanglement close to a quantum phase transition, *Nature* **416**, 608 (2002).

[27] O. Ghne, G. Tth, and H. J. Briegel, Multipartite entanglement in spin chains, *New J. Phys.* **7**, 229 (2005).

[28] M. Hofmann, A. Osterloh, and O. Ghne, Scaling of genuine multiparticle entanglement close to a quantum phase transition, *Phys. Rev. B* **89**, 134101 (2014).

[29] R. Movassagh and P. W. Shor, Supercritical entanglement in local systems: Counterexample to the area law for quantum matter, *Proc. Natl. Acad. Sci.* **113**, 13278 (2016).

[30] T. W. B. Kibble, Topology of cosmic domains and strings, *J. Phys. A: Math. Gen.* **9**, 1387 (1976).

[31] T. Kibble, Some implications of a cosmological phase transition, *Phys. Rep.* **67**, 183 (1980).

[32] W. H. Zurek, Cosmological experiments in superfluid helium?, *Nature* **317**, 505 (1985).

[33] W. Zurek, Cosmological experiments in condensed matter systems, *Phys. Rep.* **276**, 177 (1996).

[34] P. Laguna and W. H. Zurek, Density of Kinks after a Quench: When Symmetry Breaks, How Big are the Pieces?, *Phys. Rev. Lett.* **78**, 2519 (1997).

[35] A. Yates and W. H. Zurek, Vortex Formation in Two Dimensions: When Symmetry Breaks, How Big Are the Pieces?, *Phys. Rev. Lett.* **80**, 5477 (1998).

[36] J. Dziarmaga, P. Laguna, and W. H. Zurek, Symmetry Breaking with a Slant: Topological Defects after an Inhomogeneous Quench, *Phys. Rev. Lett.* **82**, 4749 (1999).

[37] A. Polkovnikov, Universal adiabatic dynamics in the vicinity of a quantum critical point, *Phys. Rev. B* **72**, 161201 (2005).

[38] W. H. Zurek, U. Dorner, and P. Zoller, Dynamics of a Quantum Phase Transition, *Phys. Rev. Lett.* **95**, 105701 (2005).

[39] B. Damski, The Simplest Quantum Model Supporting the Kibble-Zurek Mechanism of Topological Defect Production: Landau-Zener Transitions from a New Perspective, *Phys. Rev. Lett.* **95**, 035701 (2005).

[40] J. Dziarmaga, Dynamics of a Quantum Phase Transition: Exact Solution of the Quantum Ising Model, *Phys. Rev. Lett.* **95**, 245701 (2005).

[41] L. Cincio, J. Dziarmaga, M. M. Rams, and W. H. Zurek, Entropy of entanglement and correlations induced by a quench: Dynamics of a quantum phase transition in the quantum Ising model, *Phys. Rev. A* **75**, 052321 (2007).

[42] D. Sen, K. Sengupta, and S. Mondal, Defect Production in Nonlinear Quench across a Quantum Critical Point, *Phys. Rev. Lett.* **101**, 016806 (2008).

[43] J. Dziarmaga, Dynamics of a quantum phase transition and relaxation to a steady state, *Adv. Phys.* **59**, 1063 (2010).

[44] R.-Z. Huang and S. Yin, Kibble-Zurek mechanism for a one-dimensional incarnation of a deconfined quantum

critical point, *Phys. Rev. Research* **2**, 023175 (2020).

[45] I. Chuang, R. Durrer, N. Turok, and B. Yurke, Cosmology in the Laboratory: Defect Dynamics in Liquid Crystals, *Science* **251**, 1336 (1991).

[46] R. Monaco, J. Mygind, M. Aaroe, R. J. Rivers, and V. P. Koshelets, Zurek-Kibble Mechanism for the Spontaneous Vortex Formation inNb-Al/Al_xNbJosephson Tunnel Junctions: New Theory and Experiment, *Phys. Rev. Lett.* **96**, 180604 (2006).

[47] R. Barankov and A. Polkovnikov, Optimal Nonlinear Passage Through a Quantum Critical Point, *Phys. Rev. Lett.* **101**, 076801 (2008).

[48] N. Navon, A. L. Gaunt, R. P. Smith, and Z. Hadzibabic, Critical dynamics of spontaneous symmetry breaking in a homogeneous Bose gas, *Science* **347**, 167 (2015).

[49] B. Ko, J. W. Park, and Y. Shin, Kibble–Zurek universality in a strongly interacting Fermi superfluid, *Nat. Phys.* **15**, 1227 (2019).

[50] A. Keesling, A. Omran, H. Levine, H. Bernien, H. Pichler, S. Choi, R. Samajdar, S. Schwartz, P. Silvi, S. Sachdev, P. Zoller, M. Endres, M. Greiner, V. Vuletić, and M. D. Lukin, Quantum Kibble–Zurek mechanism and critical dynamics on a programmable Rydberg simulator, *Nature* **568**, 207 (2019).

[51] A. Polkovnikov, K. Sengupta, A. Silva, and M. Vengalattore, Colloquium: Nonequilibrium dynamics of closed interacting quantum systems, *Rev. Mod. Phys.* **83**, 863 (2011).

[52] C. D. Grandi, V. Gritsev, and A. Polkovnikov, Quench dynamics near a quantum critical point, *Phys. Rev. B* **81**, 012303 (2010).

[53] A. Polkovnikov, Microscopic diagonal entropy and its connection to basic thermodynamic relations, *Ann. Phys.* **326**, 486 (2011).

[54] V. Mukherjee, A. Dutta, and D. Sen, Defect generation in a spin- $\frac{1}{2}$ transverse XY chain under repeated quenching of the transverse field, *Phys. Rev. B* **77**, 214427 (2008).

[55] C. De Grandi, V. Gritsev, and A. Polkovnikov, Quench dynamics near a quantum critical point: Application to the sine-Gordon model, *Phys. Rev. B* **81**, 224301 (2010).

[56] F. Pollmann, S. Mukherjee, A. G. Green, and J. E. Moore, Dynamics after a sweep through a quantum critical point, *Phys. Rev. E* **81**, 020101 (2010).

[57] L. Pezzé and A. Smerzi, Entanglement, Nonlinear Dynamics, and the Heisenberg Limit, *Phys. Rev. Lett.* **102**, 100401 (2009).

[58] J. Haegeman and F. Verstraete, Diagonalizing Transfer Matrices and Matrix Product Operators: A Medley of Exact and Computational Methods, *Annu. Rev. Condens. Matter Phys.* **8**, 355 (2017).

[59] G. Ehlers, S. R. White, and R. M. Noack, Hybrid-space density matrix renormalization group study of the doped two-dimensional Hubbard model, *Phys. Rev. B* **95**, 125125 (2017).

[60] V. Zauner-Stauber, L. Vanderstraeten, M. T. Fishman, F. Verstraete, and J. Haegeman, Variational optimization algorithms for uniform matrix product states, *Phys. Rev. B* **97**, 045145 (2018).

[61] J. Ren, W. Li, T. Jiang, and Z. Shuai, A general automatic method for optimal construction of matrix product operators using bipartite graph theory, *J. Chem. Phys.* **153**, 084118 (2020).

[62] J. Hauschild and F. Pollmann, Efficient numerical simulations with Tensor Networks: Tensor Network Python (TeNPy), *SciPost Phys. Lect. Notes* **5** (2018).

[63] E. H. Lieb and D. W. Robinson, The finite group velocity of quantum spin systems, *Commun. Math. Phys.* **28**, 251 (1972).

[64] S. Bravyi, M. B. Hastings, and F. Verstraete, Lieb–Robinson Bounds and the Generation of Correlations and Topological Quantum Order, *Phys. Rev. Lett.* **97**, 050401 (2006).